

Chapter 3

Evolution of Multipolar Magnetic Fields in Isolated Neutron Stars

3.1 Introduction

Strong multipole components of the magnetic field have long been thought to play an important role in the radio emission from pulsars. Multipole fields have been invoked for the generation of electron positron pairs in the pulsar magnetosphere. For example, Ruderman & Sutherland (1975) model requires that the radius of curvature of the field lines near the stellar surface should be of the order of stellar radius to sustain pair production in long period pulsars. This is much smaller than the expected radius of curvature of the dipole field. Barnard & Arons (1982) showed that such small radius of curvature is only possible if the field structure has at least one dominant higher multipole. e.g. a quadrupole. Further, soft X-ray observations of pulsars show non-uniform surface temperatures which can be attributed to the presence of a quadrupolar field (Page & Sarmiento, 1996).

Magnetic multipole structure at and near the polar cap is also thought to be responsible for the unique pulse profile of a pulsar. Vivekanand & Radhakrishnan (1980) pointed out that if the dipole magnetic field curvature of the field lines vary smoothly across the polar cap then the pulse profiles should not have complicated structures as observed. However multipole components present to a small degree can significantly^a

modify the curvature of the field lines near the polar cap. This in turn can modulate the emission giving rise to random pattern as observed. Krolik (1991) noted that the complicated pulse structure observed in millisecond pulsars can be explained by invoking multipolar magnetic fields which has several reversals across the neutron stars surface which can be treated as hot spots of emission. This explanation is consistent with the large duty cycle observed in millisecond pulsars. The recent estimates that there should be several tens of sparks populating the polar cap is also best explainable if multipole fields dictate the spark geometry near the surface (Deshpande & Rankin 1998, Rankin & Deshpande 1998, Seiradakis 1998). Significant evolution in the structure of the magnetic field during the lifetime of a pulsar may therefore leave observable signatures. If the multipoles grow progressively weaker in comparison to the dipole then one can expect pulse profiles to simplify with age and vice versa.

The evolution of the magnetic fields in neutron stars in general is still a relatively open question. During the last decade, two major alternative scenarios for the field evolution has emerged. One of these assumes that the field of the neutron star permeates the whole star at birth, and its evolution is dictated by the interaction between superfluid vortices (carrying angular momentum) and superconducting fluxoids (carrying magnetic flux) in the stellar interior. As the star spins down, the outgoing vortices may drag and expel the field from the interior leaving it to decay in the crust (Srinivasan 1990). In a related model, plate tectonic motions driven by pulsar spindown drags the magnetic poles together, reducing the magnetic moment (Ruderman 1991a,b,c).

The other scenario assumes that most of the field is generated in the outer crust (for example by thermo-magnetic instability) after the birth of the neutron star (Blandford, Applegate & Hernquist 1983). The later evolution of this field is governed entirely by the ohmic decay of currents in the crustal layers. The evolution of the dipole field carried by such currents has been investigated in some detail in the recent literature (Geppert & Urpin 1994, Urpin & Geppert 1995, 1996, Konar & Bhattacharya 1997, 1999). These studies include field evolution in isolated neutron stars as well as those

accreting from their binary companions. The results show interesting agreements with observations lending some credence to the crustal picture.

In this chapter, we explore the ohmic evolution of higher order multipoles in isolated neutron stars assuming the currents to be originally confined in the crustal region. Our goal is to find whether there would be any observable effect on the pulse shape of radio emission from isolated pulsars as a result of this evolution. In section 3.2 we discuss the details of the computation, in section 3.3 we present our results and in section 3.4 discuss the implications.

3.2 The Diffusion Equation

The evolution of the magnetic field \mathbf{B} , due to ohmic diffusion, is governed by the equation (Jackson 1975) :

$$\frac{d\mathbf{B}}{dt} = -\frac{c^2}{4\pi} \nabla \times \left(\frac{1}{\sigma} \times \nabla \times \mathbf{B} \right), \quad (3.1)$$

where $\sigma(r, t)$ is the electrical conductivity of the medium which can depend on both space and time. For a constant conductivity, the diffusion equation can be written as,

$$\frac{\partial \mathbf{B}}{\partial t} = \frac{c^2}{4\pi\sigma} \nabla^2 \mathbf{B} \quad (3.2)$$

in which case the time-scale (τ) for the diffusion process would be,

$$\tau = \frac{4\sigma L^2}{\pi c^2} \quad (3.3)$$

where L is the length-scale associated with the underlying current distribution. For magnetic fields confined to neutron star crusts, L corresponds to the thickness of the crust which is of the order of a kilometer and the conductivity $\sigma \sim 10^{23} \text{sec}^{-1}$. Thus, it follows that the typical time-scale over which the fundamental mode of a dipole field would decay is of the order of $\tau \sim 10^6$ years. For multipoles of order l however, the decay time-scale is faster as the associated length-scale is smaller typically by a factor $L/2^l$. Barnard & Arons (1982) investigated the decay of the dipole and quadrupole

moments in neutron stars assuming a Cowling morlc decay (as suggested by Gunn & Ostriker, 1969). This assumption leads to exponential decay of fields where the diffusion time-scale of the quadrupole is faster than that of a dipole by a factor of 3.33. Simple-minded estimates do suggest appreciable decay in the various multipole orders of the magnetic field. As evident from equation 3.3, the decay time of any particular order is proportional to a . The density in the crust spans eight orders of magnitude and the conductivity changes sharply as a function of depth from the neutron stars surface. Studies concerning decay of dipolar fields including space and time variations of electrical conductivity suggest that the decay is not exponential. The reason being that in the diffusion process the underlying current diffuses to regions of higher conductivity, thus slowing down the decay considerably at later times. To solve equation 3.1 for varying a numerical methods have to be employed. In section 3.2.1 we discuss in detail the space and time variations of the conductivity that we use to solve equation 3.1, investigating the decay of multipolar fields.

We study the ohmic dissipation of electric currents in the outer crust of neutron stars which consists of free degenerate electrons and fully ionized ions. We assume that the magnetic field is weak enough such that it does not significantly perturb the structure or evolution of the star. Further we assume that the magnetic field in the crust is generated by some unspecified mechanism during or shortly after the neutron star's formation. Following Wendell, Van Horn & Sargent (1987) we introduce a vector potential $\mathbf{A} = (0, 0, A_\phi)$ assuming the field to be purely poloidal, such that:

$$S(r, \theta, t) = -r \sin\theta A_\phi(r, \theta, t),$$

where $S(r, \theta, t)$ is the Stokes' stream function. S can be separated in r and θ in the form :

$$S(r, \theta, t) = \sum_{l \geq 1} R_l(r, t) \sin\theta P_l^1(\cos\theta),$$

where $P_l^1(\cos(\theta))$ is the associated Legendre polynomial of degree one and R_l is the multipole radial function. From equation (3.1) we obtain :

$$\frac{\partial^2 R_l}{\partial x^2} - \frac{l(l+1)}{x^2} R_l = \frac{4\pi R_*^2 \sigma}{c^2} \frac{\partial R_l}{\partial t} \quad (3.4)$$

where $x \equiv r/R_*$ is the fractional radius in terms of the stellar radius R_* . The solution of this equation with the boundary conditions :

$$\begin{aligned} \frac{\partial R_l}{\partial x} + \frac{l}{x} R_l &= 0, \text{ as } x \rightarrow 1 \\ R_l &= 0, \text{ at } x = x_c \end{aligned} \quad (3.5)$$

for a particular value of l gives the time-evolution of the multipole of order l . Here, the first condition matches the correct multipole field in vacuum at the stellar surface and the second condition makes the field vanish at the core-crust boundary (where $r = r_c$, the radius of the core) to keep the field confined to the crust. We assume that the field does not penetrate the core in the course of evolution, as the core is likely to be superconducting.

In terms of the multipole function R_l the magnetic field, $\mathbf{B} = \nabla \times \mathbf{A}$, is given by

$$B(x, \theta, t) = \frac{1}{R_*^2} \left[-\hat{r} \sum_{l \geq 1} \frac{l(l+1)}{x^2} P_l(\cos(\theta)) R_l(x, t) + \hat{\theta} \sum_{l \geq 1} P_l^1(\cos(\theta)) \frac{1}{x} \frac{\partial R_l}{\partial x} \right] \quad (3.6)$$

and the underlying current distribution, \vec{j} is:

$$\vec{j} = \frac{c}{4\pi} \nabla \times \mathbf{B} \quad (3.7)$$

3.2.1 Crustal Physics

The rate of ohmic dissipation in the crust is determined by the electrical conductivity a in the crust. The crust of the neutron star consists of relativistic, Fermi-degenerate free electron gas plus a non-relativistic, non-degenerate liquid or crystal of ions. In the crust of the neutron star both density and temperature vary with radius. In regions close to the surface where the temperature $T > T_m$ (T_m is the melting temperature) the ions are in the liquid or gaseous phase. In deeper layers where $T_m > T$, the ions are crystallized. The condition for the melting or crystallization of a crustal material depends on the ratio (Γ) of the Coulomb energy to the thermal energy of the crystal, which is the Lindeman criterion for a one component plasma. On the basis of this criterion Slattery et al (1982), have shown that $\Gamma = 171$ at, the melting point. For a crystal of ionic species Z and lattice spacing a , which is at a temperature T , the ratio

$\Gamma = (Z^2 c^2 / a) / k_B T$, where k_B is the Boltzmann constant. The lattice spacing a can be written as,

$$a = \left[\frac{4\pi}{3} \right]^{-1/3} \left[\frac{\rho}{A} \right]^{-1/3} m_p^{-1/3} \quad (3.8)$$

where m_p is the proton mass and A is the mass number of the ion. Thus the temperature T and Γ are related by,

$$T = 0.227 \times 10^8 Z^2 \frac{(\rho_6/A)^{1/3}}{\Gamma} K \quad (3.9)$$

where ρ_6 is the density in units of 10^6 g cc^{-3} . The transport properties in the liquid state is determined by electron-ion collisions. We use the conductivity of the liquid layer as suggested by Yakovlev & Urpin (1980):

$$\sigma_{\text{liquid}} = 8.53 \times 10^{21} \frac{x^3}{Z \gamma_{\text{coulomb}} (1 + x^2)} \quad (3.10)$$

where γ_{coulomb} is the Coulomb logarithm and x is given by $(Z/\rho_6)^{1/3}$. A simple interpolation formula for γ_{coulomb} was proposed by Yalcovlev & Urpin (1980):

$$\gamma_{\text{coulomb}} = \ln \left[(4Z)^{1/3} (1 + 2/\Gamma)^{1/2} \right] - \frac{x^2}{2(1 + x^2)}. \quad (3.11)$$

Detailed calculations by Itoh et al. (1983) have confirmed that for $Z \geq 2$, the Coulomb logarithm is well approximated by equation 3.11, with an error $\leq 10 \%$ which is sufficient for our purpose. It is to be noted that σ_{liquid} is practically independent of temperature. For given Z, A, T and ρ_6 , we find Γ using equation 3.9. For $\Gamma < 171$, we use the conductivity as given by equation 3.10.

In the solid crust the conductivity arises due to electron-phonon scattering. Excepting at very low temperatures, the Umklapp process dominates mainly due to presence of the longitudinal acoustic mode in the phonon spectrum. We use the phonon scattering conductivity (σ_{ph}) for the pure crystalline phase from the results obtained by Itoh et nl. (1984) where

$$\sigma_{\text{ph}} = 1.24 \times 10^{20} \frac{x^4 (u^2 + 0.0174)^{1/2}}{u T_8 (1 + 1.018 x^2) I_\sigma} \quad (3.12)$$

Here T_8 is the temperature in units of 10^8 , $u = \frac{2\pi}{9} (\log \rho - 3)$, ρ_6 is the density in units of 10^6 g cm^{-3} and I_σ is a function of density, Z and the atomic number A . The crystallized crust is liltely to have structural defects like impurities, dislocations, cracks and so on.

For lower temperatures, the electron scattering on defects may be more effective than on phonons. We use the conductivity for such scattering (σ_{imp}) given by Yakovlev & Urpin (1980) as

$$\sigma_{\text{imp}} = 8.53 \times 10^{21} xZ/Q \quad (3.13)$$

where the effect of impurities on the conductivity is usually parametrised by a quantity Q , defined as $Q = \frac{1}{n} \sum_i n_i (Z - Z_i)^2$, where n is the total ion density, n_i is the density of impurity species i with charge Z_i , and Z is the ionic charge in the pure lattice (Yakovlev & Urpin 1980). In the literature Q is assumed to lie in the range 0.0 - 0.1. But statistical analyses indicate that the magnetic field of isolated pulsars do not undergo significant decay during the radio pulsar life time (Bhattacharya et al 1992, Hartman et al 1997, Mukherjee & Kembhavi 1997). It has been shown (Konar 1997) that to be consistent with this impurity values in excess of 0.01 are not allowed in the crustal model. The effective conductivity of the solid crust is thus given by

$$\frac{1}{\sigma} = \frac{1}{\sigma_{\text{ph}}} + \frac{1}{\sigma_{\text{imp}}}$$

Knowledge about the the various parameters like Z , a , ρ_6 etc. requires accurate knowledge of the neutron star's structure as well as composition. We obtain the mass and density profile of the neutron star by integrating the relativistic hydrostatic pressure balance equation (Tolman-Oppenheimer & Volkoff 1939):

$$\frac{dP(r)}{dr} = - \frac{G \left(M(r) + \frac{4\pi P(r)}{c^2} \right) \left(\rho(r) + \frac{P(r)}{c^2} \right)}{r^2 \left(1 - \frac{2GM(r)}{r^2 c^2} \right)} \quad (3.14)$$

where $P(r)$, $M(r)$ and $\rho(r)$ are the pressure, mass and density at, a distance r from the stellar center, G is the gravitational constant and c is the speed of light and the mass equation:

$$\frac{dM(r)}{dr} = 4\pi r^2 \rho(r) \quad (3.15)$$

Using the equation of state of Wiringa, Fiks & Fabrocini (1988) for $\rho > 2.8 \times 10^{14} \text{gcc}^{-3}$ and Negele & Vautherin (1973) and Baym Pethick & Sutherland (1971) at lower densities (see section 1.8). The composite equation of state for the entire density

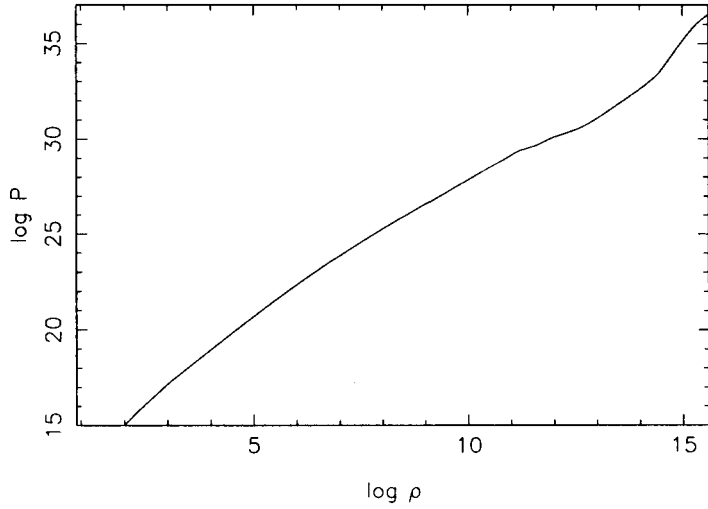


Figure 3.1: Pressure vs. Density. The above figure is adopted from Konar 1997.

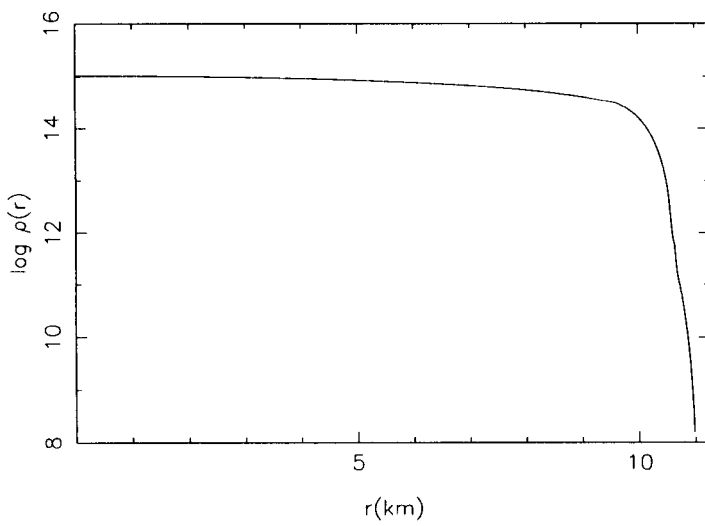


Figure 3.2: Density vs. Radius for a $1.4 M_{\odot}$ neutron star. The above figure is adopted from Konar 1997.

range is shown in figure[3.1]. To do the structure calculations we have used the numerical methods and the programs developed by Konar (1997, also see Konar & Bhattacharya, 1999). We solve equations[3.14] and [3.15] starting from a particular central density and pressure at zero radius and zero mass, and integrating outwards using a fourth order Runge-Kutta scheme. The resultant density profile of a $1.4 M_{\odot}$ neutron star is shown in figure [3.2].

The next important factor in determining the conductivity of the neutron star is the temperature of the crust. In absence of impurities the scattering of crustal electrons come entirely from the phonons in the lattice (Yakovlev & Urpin 1980) and the number density of phonons increases steeply with temperature. The thermal evolution of the crust therefore plays an important role in the evolution of the magnetic field. The thermal evolution of a neutron star has been computed by many authors, and it is clearly seen that the inner crust ($\rho > 10^{10} \text{gcm}^{-3}$) quickly attains an isothermal configuration after birth. At outer regions of the crust, the temperature follows an approximate relation,

$$T(\rho) = \left(\frac{\rho}{\rho_b} \right)^{1/4} T_i, \quad \rho \lesssim \rho_b \quad (3.16)$$

where T_i is the temperature of the isothermal inner crust and ρ_b is the density above which the crust is practically isothermal. As the star cools, larger fraction of the crust starts becoming isothermal, with ρ_b being approximately given by,

$$\rho_b = 2.5 \times 10^7 \left(\frac{T_i}{10^9} \right)^{1.8} \quad (3.17)$$

The relations 3.16 and 3.17 above have been obtained by fitting to the radial temperature profiles published by Gudmundsson, Pethick & Epstein (1983). as displayed in figure 3.3. For the time evolution of T_i we use the results of Urpin & van Riper (1993) for the case of standard cooling (the crustal temperature T_m in their notation corresponds to T_i above), shown in figure 3.4. The variation of the electrical conductivity in the crust with density for the case where $T_i = 10^{4.5} K$ and for various values of impurity strength is shown in figure[3.5].

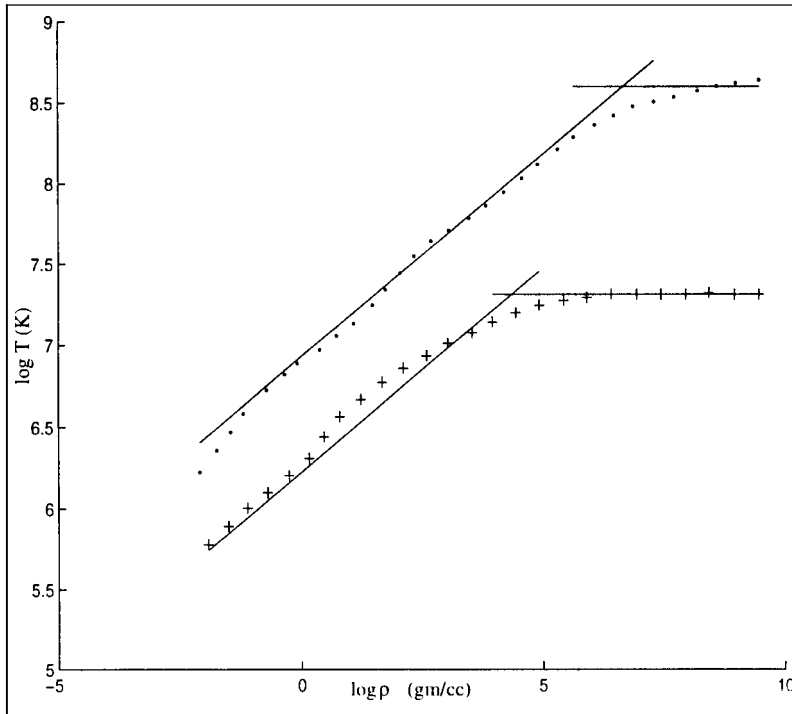


Figure 3.3: The above plot shows the fitted relations 3.16 and 3.17 to the radial temperature profiles (points with crosses and dots) published by Gudmundsson, Pethick & Epstein (1983). The points with crosses correspond to surface temperature of $10^{5.5} \text{K}$ and with dots to $10^{6.5} \text{K}$ while the surface gravity is 10^{14}cm s^{-2} for both the cases. The temperature of the isothermal crust T_i is denoted by the horizontal lines and the temperatures of the outer crust $T(\rho)$ is denoted by the sloped lines. The intersection of these lines gives the ρ_b for a given surface temperature.

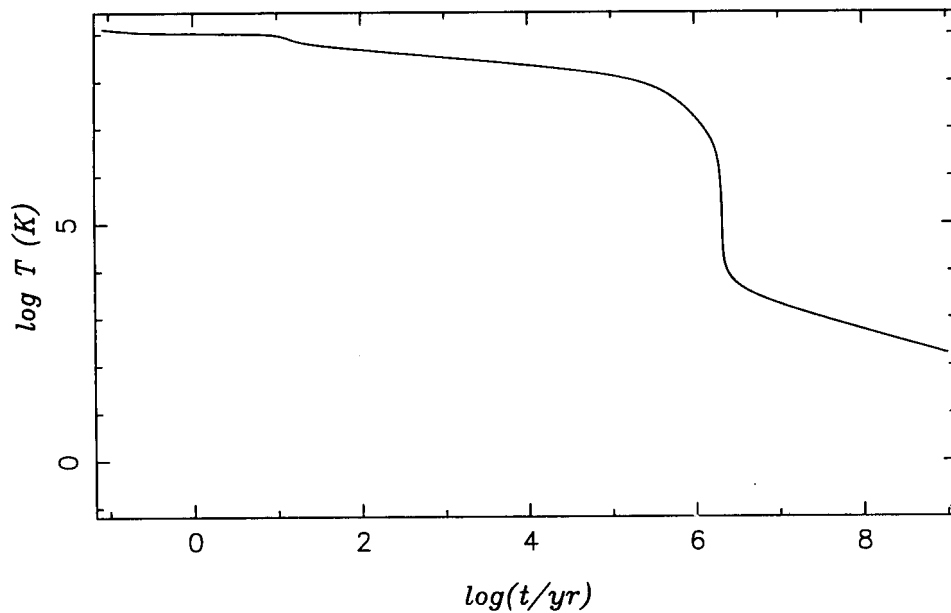


Figure 3.4: Evolution of the temperature of the inner crust (T_i) for the rise of standard cooling model of neutron star.

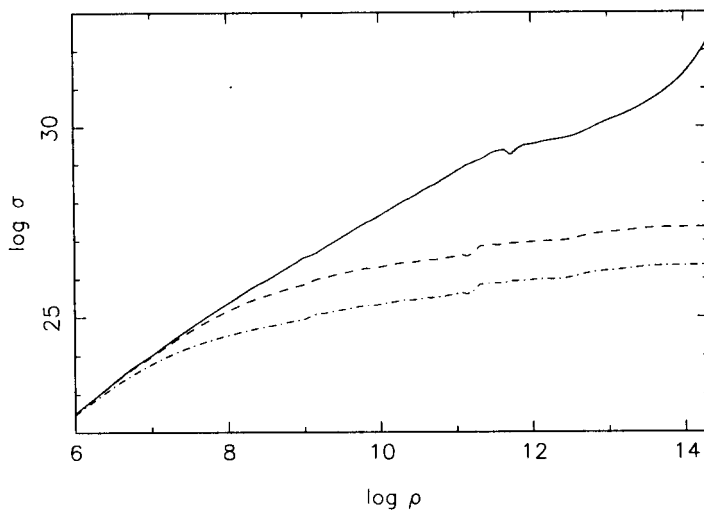


Figure 3.5: Variation of the electrical conductivity with density in the crust of a cool neutron star. The solid, dashed and dashed-dotted curves correspond to $Q = 0.0, 0.01$ and 0.1 respectively. The surface temperature for all the curves is $10^{4.5}$ K. The above figure is adopted from Konar 1997.

3.2.2 Numerical Scheme

The aim of our computation is to solve equation [3.4] to obtain $R_l(r, t)$ for all times. We solve the equation [3.4] in terms of the fractional radius x . Let us introduce a function $D(x, t)$ where,

$$D(x, t) = \frac{c^2}{4\pi\sigma(x, t)R_*^2}. \quad (3.18)$$

Thus equation (3.4) takes the form

$$\frac{\partial R_l}{\partial t} = D(x, t) \left(\frac{\partial^2 R_l}{\partial x^2} - \frac{l(l+1)}{x^2} R_l \right) \quad (3.19)$$

To solve the above equation we use the Crank-Nicholson method of differencing. The differenced form of the equation is,

$$\frac{R_j^{n+1} - R_j^n}{\text{lit}} = D_j^{n+1/2} \left(\frac{R_{j+1}^{n+1} - 2R_j^{n+1} + R_{j-1}^{n+1} - 2R_j^n + R_{j-1}^n}{2(\delta x)^2} - l(l+1) \frac{R_j^n}{x_j^2} \right) \quad (3.20)$$

where δt and δx represent the time interval and size of the space-grid and $R \equiv R_l$. The superscript n stands for the n^{th} time-step and the subscript j stands for the j^{th} space-grid of integration. The function $D(x, t)$ depends on $\sigma(x, t)$ which varies with both density (and hence with the fractional radius x) and time in the manner discussed in the section [3.2.1]. To incorporate this feature we use the time-averaged value of the function between two neighbouring intervals (as suggested by the index $n + 1/2$) at each time step. Since D is a slowly-varying function over the time intervals chosen for the integration no significant error is introduced due to this assumption. Rearranging equation (3.20) with the $(n + 1)$ index on the left hand side and n^{th} index on the right hand side one obtains,

$$A_j R_{j-1}^{n+1} + B_j R_j^{n+1} + C_j R_{j+1}^{n+1} = E_j R_{j-1}^n + F_j R_j^n + G_j R_{j+1}^n \quad (3.21)$$

where,

$$\begin{aligned} A_j &= -1 \\ B_j &= \frac{1}{D_j^{n+1/2}} \frac{2(\delta x)^2}{\delta t} + 2 \\ C_j &= -1 \end{aligned}$$

$$F_j^n = \frac{1}{D_j^{n+1/2}} \frac{2(\delta x)^2}{\delta t} - l(l+1) \frac{(\delta x)^2}{x_j^2} - 2$$

$$G_j = 1$$

The next step is to apply the boundary conditions as given by equation (3.5). In the differenced form the boundary conditions manifest as $R_1 = 0$ for the core-crust boundary and $R_J = \frac{R_{J-1}}{(1+l\delta x)}$ at the surface where the space-grid index j runs from 1 to J . Writing equation (3.21) componentwise the first and the last equations drops out by virtue of the boundary conditions. Making another set of substitution as $u_k = R_{k+1}$ for $1 \leq k \leq J - 2$, equation (3.21) can be written componentwise as,

$$B'_1 u_1^{n+1} + C'_1 u_2^{n+1} = F'_1 u_1^n + G'_1 u_2^n$$

$$A'_k u_{k-1}^{n+1} + B'_k u_k^{n+1} + C'_k u_{k+1}^{n+1} = E'_k u_{k-1}^n + F'_k u_k^n + G'_k u_{k+1}^n, \quad \text{for } k = 2, K - 1 \quad (3.22)$$

$$A'_K u_{K-1}^{n+1} + (B'_K + C'_K) u_K^{n+1} = E'_K u_{K-1}^n + (F'_K + \frac{G'_K}{(1-l\delta x)}) u_K^n$$

where the primed quantities are related to the unprimed quantities given by equation (3.22) as $X'_j = X_{j+1}$ and X can be A, B, C, E, F and G respectively. Equation [3.23] is in the tridiagonal form and we solve it by using the subroutine ‘tridag’ as available from the numerical recipes (Press et al. 1993).

We assume the initial radial form of the radial function R_l to be given by:

$$R_l(x, 0) = \frac{1}{\sqrt{2\pi}} \int_{-\infty}^x e^{-\frac{(x'-x_o)^2}{2x_w^2}} dx' \quad (3.23)$$

as used by Bhattacharya & Datta (1996, see also Konar & Bhattacharya 1997). This is an error function which varies from unity to nearly zero within a width x_w around $x = x_o$ (see figure [3.6]). This profile contains the depth x_o and the width x_w of the current configuration as input parameters and we vary them to check the sensitivity of the result to these parameters.

3.3 Results

In figures [3.7] and [3.8] we plot the evolution of the various multipole components of the magnetic field, assuming the same initial strength for all, with time due to pure

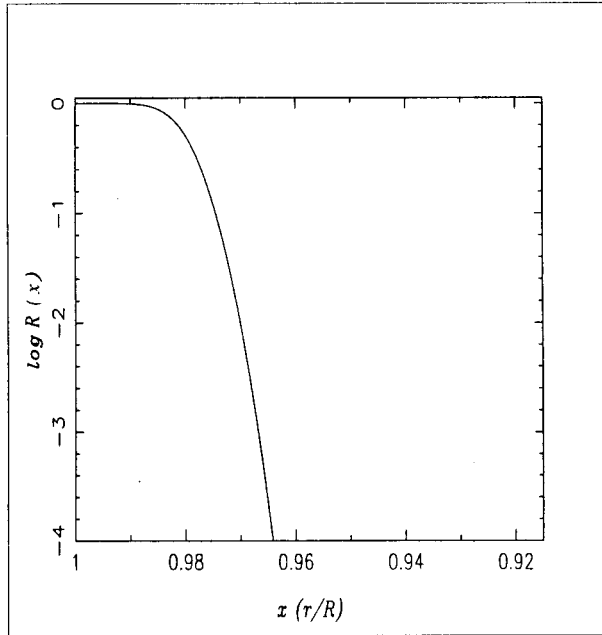


Figure 3.6: The initial radial profile R_l (equation 3.23) centered around $x = 0.98$ which corresponds to $\rho = 10^{11}$ g/cc and width $x_w = 0.006$.

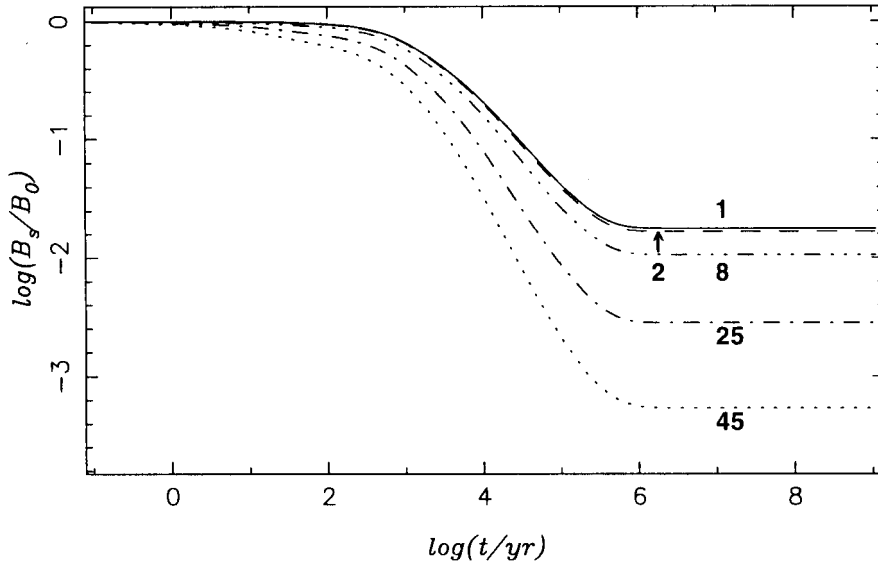


Figure 3.7: The evolution of the surface magnetic field for various multipoles due to pure diffusion. The numbers next to the curves correspond to respective orders of multipole. All the curves correspond to $Q = 0.0$ and a depth of current concentration at $x_0 = 0.98$ i.e., a density of $\rho = 10^{11}$ g/cc.

diffusion in an isolated neutron star of $1.4 M_{\odot}$. It is evident from the figures that except for very high multipole orders ($l \gtrsim 25$) the reduction in the field strength is very similar to that of the dipole component.

Krolik (1991) and Arons (1993) conjectured that except for multipoles of order $l \gtrsim R_{*}/\Delta r$ the decay rates would be similar due to the finite thickness Δr of the crust over which the current is confined. The evolution plotted in figure [3.7] assumes that $\Delta r = 1.2$ km for which $R_{*}/\Delta r \sim 8$. However it is seen from figures [3.7] and [3.8] that significant decay occurs only for $l \gtrsim 25$, much greater than $R_{*}/\Delta r$. This is most likely caused by steep increase in conductivity towards the interior.

To test the sensitivity of our results on the impurity concentration of the crust and the density at which the initial current is concentrated we have evolved models with various values of these parameters. The results are displayed in figures [3.9] and [3.10] where we plot the ratio of the dipole to higher multipoles at an age of 10^7 years. It is seen that the results are insensitive to these parameters, particularly for low orders of multipoles of interest.

3.4 Discussion

The presence of strong multipole fields near the stellar surface would modify the radius of curvature of the local field lines substantially, and may be responsible for creating an "illumination pattern" of the radio emission beam which is unique to every pulsar. While the magnetic field structure in radio emission region, which is located far away from the surface, may be much closer to dipole owing to the substructure in integrated pulse profiles (cf. section 1.3.2). If the strength of the multipole fields evolve significantly with respect to the dipole, one would expect to see a corresponding change in the structure of the pulse profiles. In a typical pulsar the polar cap, defined by the base of the open field lines, occupies $\sim 0.01\%$ of the surface area of the star. To contribute to pulse substructure, the relevant multipoles should have a few reversals across the polar

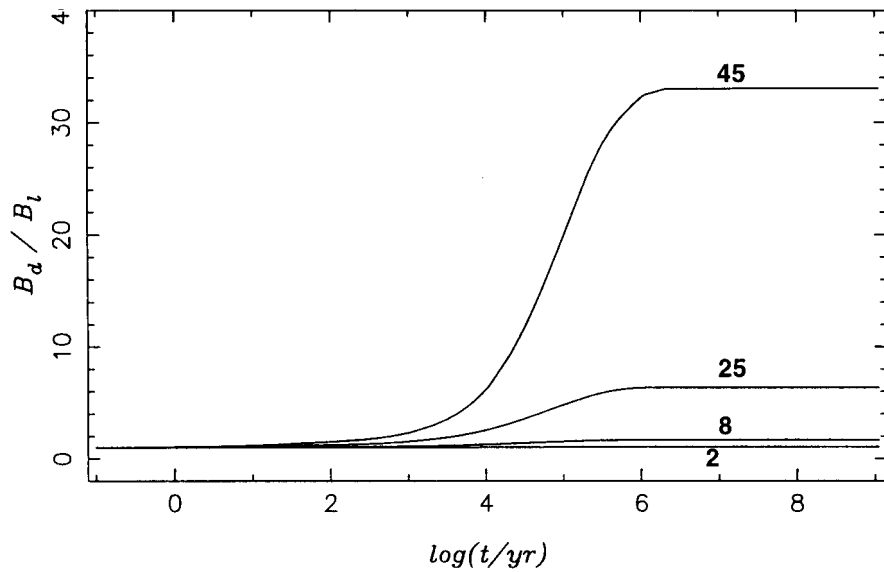


Figure 3.8: The ratio of the dipole surface field to the multipole field is plotted as a function of age. The numbers next to the curves correspond to respective orders of multipole. All the curves correspond to $Q = 0.0$ and a depth of current concentration at $x = 0.98$ i.e., a density of $\rho = 10^{11} \text{ gm/cc}$.

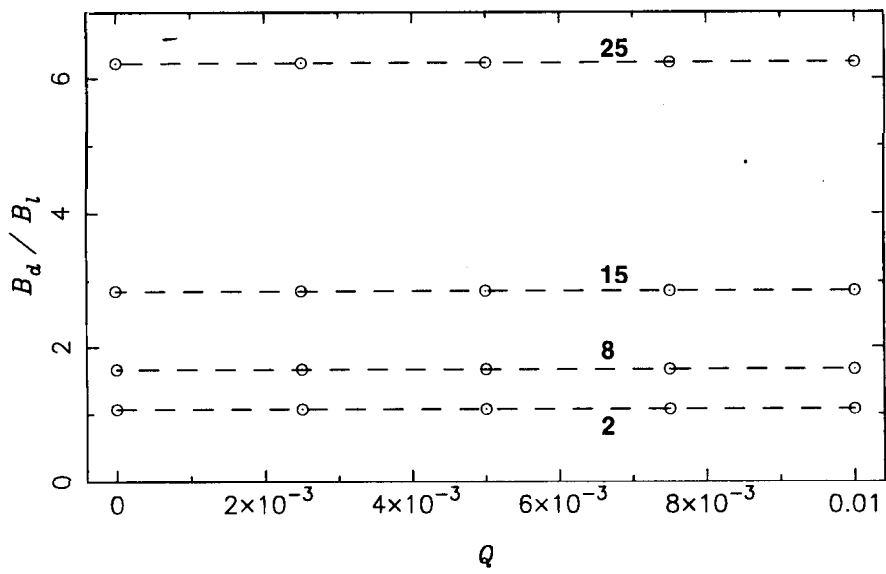


Figure 3.9: The ratio of the dipole surface field to that of the multipoles at 10^7 years as a function of Q . The numbers next to the curves correspond to respective orders of multipole. All curves correspond to a depth of $x = 0.98$ corresponding to a density of $\rho = 10^{11} \text{ gm/cc}$, at which the initial current is concentrated.

Pulsar Bname	number of components	log(t) years
0329+54	5	6.74
0355+54	5	5.75
0740-28	7	5.2
0823+26	3	6.69
0919+06	2	5.7
0950+08	4	7.24
1133+16	3	6.7
1642-03	3	6.54
1706-16	5	6.21
1845-01	3	6.3
1929+10	6	6.49
2020+28	3	6.46
2021+51	4	6.40
2045-16	3	6.45
2310+42	4	7.68
2319+60	3	6.71

Table 3.1: The above table illustrates the number of components as computed by Kramer et al (1994) as a function of the pulsar spin-down age. See text for detail.

cap. This suggests that the multipole order of relevance is five or more (a multipole of order l has 2^l reversals across the surface). On the other hand if the multipole order is very large ($l > l_{max}$), the fine structure produced by them will be too small to be resolved in observations. The best time resolution achieved so far, of order a microsecond, limits l , to $\lesssim 20$. The major contribution to the observed substructure of pulse profiles would therefore come from multipole orders ~ 5 to l_{max} . However, we find that, the evolution of multipoles of such orders is very similar to that of the dipole (figures 3.7, 3.8), in the age range 10^5 to 10^8 years, where the vast majority of pulsars are seen. Therefore no significant evolution is expected in the pulse shape due to evolution of the multipole structure of the field.

An observational investigation of the pulse structure has been carried out recently by Kramer et al (1994). They decompose the integrated pulse profiles of several pulsars into components using multi-gaussian fits (Kramer 1994), and list the number of components, which is a measure of the complexity of pulse profiles. Their result is reproduced in table [3.1], where we list the name of the pulsar, spindown age and the

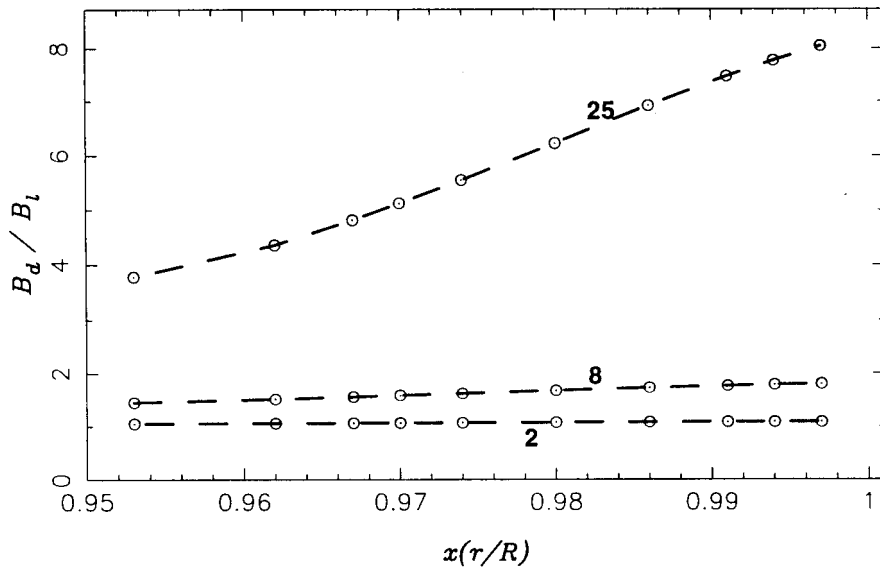


Figure 3.10: The ratio of the dipole surface field to that of the multipoles at 10^7 years as a function of depth of initial confinement of the magnetic flux. The points marked in the plots here correspond to confinement densities $\rho = 10^{13.5}, 10^{13}, 10^{12.5}, 10^{12}, 10^{11.5}, 10^{11}, 10^{10.5}, 10^{10}, 10^{9.5}, 10^9 \text{ g cc}^{-3}$. The numbers next to the curves indicate multipole orders. All curves correspond to $Q = 0$.

number of components. Clearly there is no obvious correlation between the number of components in the pulse profile and the spin down age, suggesting that the profile complexity does not evolve with age. This is, however, only a preliminary indication, and a more systematic and detailed study, taking into account the impact parameter β (see chapter 2) of the line of sight with respect to the magnetic axis, with reference to the opening angle ρ , will be necessary to confirm this result.

At present therefore, it can be said that there is no evidence of the evolution of the complexity in pulse shapes. This is consistent with the lack of significant evolution in multipole structure expected from our calculations.

As mentioned in section 3.1, in the Ruderman & Sutherland (1975) model of pulsar emission, one needs low-order multipoles to sustain pair production in long period pulsars. According to this model, pulsar activity due to lack of sufficient gap voltage (section 1.7) would cease if the period of the pulsar exceeds a critical value,

$$P_{\text{crit}} = 1.7 B_{12}^{8/13} \kappa^{-4/13} \text{ sec} \quad (3.24)$$

where κ (in units of 10^6 cm) is the radius of curvature of the open field line near the polar cap. To explain the existence of long period pulsars (up to $\sim 8.5 \text{ sec}$), κ has to be much smaller than that can be achieved from a dipolar field geometry. This indicates the necessity of strong multipole field at the stellar surface. Barnard & Arons (1982) suggest that at least a quadrupole component of the field in addition to a dipole is required to explain the presence of long period pulsars. It would be a matter of concern, therefore, if the multipole components of the magnetic field decay too quickly. But as shown by our results, the low order multipoles relevant in this context do not decay significantly faster than the dipole, therefore preserving the small value of κ through the life of a radio pulsar. Our result corresponds to the case where the magnetic field is initially located in the outer crust of the star, where the fastest evolution can be expected. If the field is anchored deeper in the star to begin with, then the evolution will be even slower than what is presented here. It seems clear therefore, that simplification of the magnetic field structure would not be a factor contributing to the cessation of pulsar activity.

In conclusion, our results indicate that for a crustal model of the neutron star magnetic field there would be no significant change in the multipolar structure with age. This fact seems to be corroborated by observations: studies identifying multiple components in pulse profiles (Kramer et al, 1994) show that the number of components does not vary with the age of the pulsar. Thus the evolution of the multipolar structure of the magnetic field is unlikely to leave any observable signature on pulsar emission. In contrast, substantial evolution of pulse profiles was suggested by Ruderman (1991a,b,c) following the plate-tectonics model. According to this model while the neutron star is spinning down (or up) the neutron star's crust is subjected to strong stresses. Cracks, and crustal plate move, due to strong stresses imposed by multiply-pinned crustal superfluid vortices (Anderson & Itoh 1975, Ruderman 1976, Alpar et al. 1984a,b). Spin-down is expected to result in migration of plates towards the equator, which can bring magnetic poles together, resulting in a major change in magnetic geometry. This should also be reflected in the shape of radio pulses, the evidence of which has not been found.